

RESEARCH

Open Access



# Innovative K-band slot antenna array for radar applications

Shaza M. Elnady<sup>1\*</sup> , Anwer S. Abd El-Hameed<sup>1,2</sup> and Eman G. Ouf<sup>1</sup>

\*Correspondence:  
shazaelnady@eri.sci.eg

<sup>1</sup> Electronics Research Institute,  
Cairo, Egypt

<sup>2</sup> Center for Northeast Asian  
Studies, Tohoku University,  
Sendai, Japan

## Abstract

This article introduces a novel microstrip slot antenna array (SAA) configuration for radar applications. The proposed antenna is specifically designed for operation in the K-band, spanning from 23 to 24.3 GHz. The antenna structure comprises two substrates: the feed network and ground plane are on the bottom substrate, and the radiating slots are on the top layer of the first substrate. The incorporation of a unique grid feed configuration, featuring 50 Ohm center excitation for the first time, improves the feed mechanism of the microstrip SAA. This innovation contributes to achieving a compact size and high gain. To enhance the side lobe level, the design incorporates a substrate-integrated waveguide-backed cavity, which significantly reduces surface waves. The SAA consists of 25 radiating elements with a gain of 14 dBi. In the elevation and azimuth planes, the half-power beamwidths are measured at 12.1° and 69.1°, respectively. The proposed antenna array's measured impedance bandwidth ranges from 23.15 to 24.75 GHz, guaranteeing a reflection coefficient ( $S_{11}$ ) of less than  $-10$  dB. The suggested antenna's applicability for automotive multi-input multi-output radar has been validated.

**Keywords:** HPBW, K-band, Radar, SAA, SIW, SLL

## Introduction

Radar is a method of utilizing reflected electromagnetic waves to determine the position, distance, orientation, and speed of an object or target [1]. Its original purpose was to aid air defense against German aircraft during the Second World War. Since then, its scope has broadened significantly to encompass various civil and commercial applications such as managing traffic, predicting weather, and observing Earth [2]. More recently, it has become popular in the automotive and industrial sectors for collision avoidance, cruise control, traffic monitoring, and motion detection. Radar systems can be categorized according to the waveform of the transmitted signals into two types: continuous-wave (CW) radar and pulse radar [3, 4]. Pulse radar uses pulse signals with shorter pulse widths to achieve better distance resolution but requires high power and wide frequency bandwidth, limiting its use mainly to military applications. In contrast, CW radar encompasses different types such as single-tone CW, frequency shift keying (FSK), and frequency-modulated CW (FMCW).

Detecting the velocity of an object through CW radar involves utilizing the frequency change caused by the Doppler effect when the object reflects the electromagnetic wave [5]. Nevertheless, this radar type lacks the ability to determine the distance of an object or the velocity of a stationary object. In contrast, FSK radar can gauge the distance and speed of a moving object by transmitting diverse discrete frequencies but falls short in determining the distance to a stationary object [6]. FMCW radar, employing a voltage-controlled oscillator (VCO), can compute the frequency shift between received and transmitted frequencies through a linearly modulated transmitted frequency. Consequently, FMCW radar excels at measuring the speed and distance of a moving object and determining the distance to a stationary object [7]. These advantages position FMCW radar as the most precise and widely adopted method. Furthermore, FMCW radar offers several advantages over pulsed radar for automotive applications. It provides higher range resolution and better velocity measurement accuracy, thanks to continuous frequency variation, which allows for precise detection of multiple targets. Additionally, FMCW radar consumes less power and is less susceptible to interference, making it more suitable for the demanding environment of automotive radar systems.

In the field of automotive millimeter-wave radar, there are three primary frequency bands that are used: 24, 77, and 79 GHz [8]. The 24 GHz band is employed for short-range functions that cover distances of up to 300 m, such as detecting blind spots, alerting about rear cross-traffic, and avoiding collisions. The 77 GHz band, on the other hand, is utilized for longer-range purposes that extend up to 250 m, which includes adaptive cruise control and warning systems for forward collisions. The 79 GHz band is specifically designated for short-range applications that require high-resolution detection. Additionally, it is expected that in the near future, the higher millimeter-wave band (100–300 GHz) or the sub-terahertz band (100–1000 GHz) will be used for radar applications that require even greater resolution.

The microstrip antenna is suitable for automotive radar systems because it is cost-effective, easily fabricated and integrated, and has a low profile. However, it also has some disadvantages, such as low gain and narrow bandwidth. To overcome these limitations, various techniques have been developed to enhance the gain of microstrip antennas, including the use of shorting pins [9, 10], parasitic elements [11], dielectric superstrates [12, 13], frequency-selective surfaces [14], artificial magnetic conductors [15], and metamaterials [16], as well as loading split-ring resonators [17, 18]. While these approaches can significantly increase the realized gain, they often require complex structures and high accuracy, which can increase the cost and size of the antenna.

An alternative method to achieve higher gain is by forming an array. Previous studies have presented two transmit array structures that have shown a realized gain increase of at least 7 dB compared to a directional antenna source, as well as achieving a relatively narrow beamwidth [19, 20]. The types of array antennas commonly used for 24 GHz FMCW automotive radar include patch antennas [21, 22], slot antennas [23, 24], and grid antennas [25]. The SAA is a potential option for scanning frequencies in the higher microwave and millimeter-wave ranges [26]. Furthermore, the SIW technique facilitates the straightforward fabrication of various rectangular waveguide structures. Moreover, studies have demonstrated the efficient radiation capabilities of SIW slot array antennas in the higher microwave and millimeter-wave frequency ranges [27–30]. The discussed

configuration is capable of addressing both near and far ranges. While the previously mentioned papers explored various antenna configurations, they either overlooked the antenna SLL or encountered challenges with low antenna gain.

In this paper, a broad-spectrum microstrip SAA activated by a coaxial-fed probe employing a grid-feeding network at 24 GHz is specifically designed for automotive radar applications. Our design innovation lies primarily in the novel feeding method, which employs a grid configuration combined with a SIW cavity backing. The slot antenna elements are arranged symmetrically along the x and y axes, with optimized inter-element spacing of  $\lambda/2$  to achieve low side lobe levels (SLL). The SIW cavity backing plays a crucial role in minimizing surface wave currents, thereby significantly reducing the SLL to values below  $-23$  dB in both the XZ and YZ planes. The proposed design features a straightforward center feed, a radiation pattern oriented toward the broad-side, and a limited number of optimization parameters. The measured results confirm the accuracy of the simulated model and further validate the performance of the SAA. This information is crucial for applications that require high gain and low reflection within the specified frequency range, such as wireless communication systems or radar systems operating in the 23.15–24.75 GHz frequency band. The remainder of the paper is organized as follows: The MIMO radar and its significance in relation to traditional radar systems are discussed in Section “MIMO radar.” Section “Antenna design” presents the recommended antenna, along with its design geometry and feeding network. A comparison of the simulated and measured findings is presented in Section “Experimental results of the SAA.” The suggested MIMO radar, MIMO antenna configuration, and radar image reconstruction were covered in Section “Proposed MIMO radar.” The conclusion is finally presented in Section “Conclusion.”

### **MIMO radar**

In the field of automotive radar, the incorporation of MIMO radar technology, especially operating in the K-band frequency, signifies a notable advancement toward improving detection and sensing capabilities. A MIMO radar stands out from conventional radar systems in that it employs numerous antennas for both transmission and reception, allowing for the simultaneous transmission of multiple waveforms.

Constructing an antenna array with a low SLL typically requires element spacing of less than half a wavelength, which is often impractical in real-world scenarios. However, the use of a virtual antenna array approach offers a solution to this challenge. The virtual array concept refers to how signals in MIMO systems are affected by the multiplication of the radiation patterns when transmitted from one antenna and received by another. By carefully arranging the MIMO elements so that each transmit/receive radiation pattern null is aligned with the receive/transmit peak, the SLL can be significantly reduced. This concept will be further elaborated upon later in the discussion. The convolution of the respective excitation distributions results in the superposition of observations, effectively creating a synthetic antenna array. This configuration leads to a notable reduction in the SLL of the virtual array, offering improved resilience against unwanted clutter [31].

For a better understanding, assume  $n$  and  $m$  transmit and receive antennas, respectively, are used to construct a MIMO radar system. To determine the area covered by the antenna, we analyzed a hypothetical antenna with a central wavelength of  $\lambda$ . The

location of the transmit (Tx) antennas is noted as  $x_m$ , while the receive (Rx) antennas are positioned at  $y_n$ . Assuming that there is an object at a distance  $r$  from the automotive radar, the virtual MIMO array factor ( $AF_{\text{MIMO}}$ ) is obtained by multiplying the Tx array factor ( $AF_{\text{Tx}}$ ) by the beam factor ( $AF_{\text{Rx}}$ ), as mentioned in Eq. (1), [8].

$$AF_{\text{MIMO}}(\vec{e}) = AF_{\text{Tx}}(\vec{e})AF_{\text{Rx}}(\vec{e}) = \frac{1}{N}e^{i\frac{4\pi}{\lambda}r} \sum_{m,n} \left( \exp\left(\frac{x_m + y_n}{2}\right) \cdot \vec{e} \right) \quad (1)$$

The antenna half-power points ( $-3$  dB) of the radiation pattern are used to define the angular resolution. If there is a distance between two identical targets at the same distance that is higher than the  $-3$  dB beamwidth, the objects can be discriminated by angle. If, in the driving scenario shown in Fig. 1, two identical cars are positioned at a slant range  $R$  from the sensor and are separated by a distance,  $d$ , the necessary angular resolution can be ascertained by applying the following expression:

$$\Delta\theta = \sin^{-1}\left(\frac{d}{R}\right) \quad (2)$$

This parameter holds significant importance in scenarios where a vehicle must determine if the lane between two cars is occupied. Achieving this task poses a challenge for currently deployed automotive radars, which typically attain only a few degrees of angular resolution while sacrificing a wide field of view (FOV) and facing ambiguity in angles (permitting targets from multiple angles to overlap). Fortunately, this issue can be addressed with a coherent MIMO radar system.

This article introduces an alternative MIMO antenna setup using the SAA geometry instead of the conventional patch antenna commonly used in K-band commercial systems. The suggested antenna provides numerous advantages, including reliability, exceptional radiation patterns, easy portability, cost effectiveness, and compliance with the radiation pattern standards for automotive radar antennas discussed earlier in the introduction.

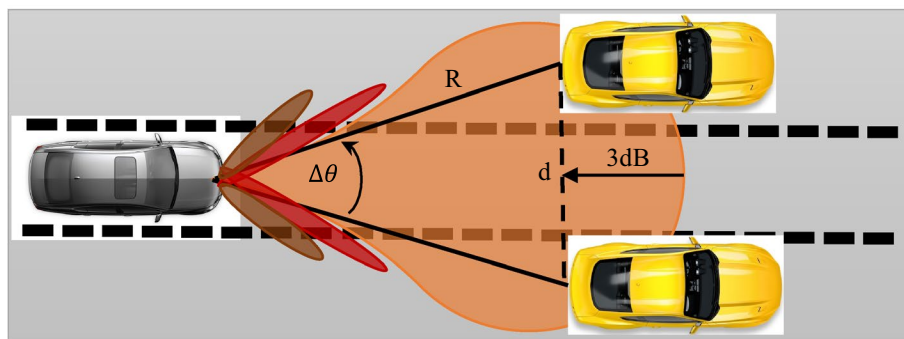


**Fig. 1** The angular resolution of a radar determined by  $-3$  dB beamwidth of the main lobe

## Antenna design

This section focuses on the design of the microstrip SAA with a SIW cavity backing. Enhancements in the antenna characteristics are examined by investigating the integration of a grid configuration feeding network in conjunction with the SAA. To fulfill the requirements of the radiation pattern for automotive radar applications, a total of 25 antenna elements have been chosen.

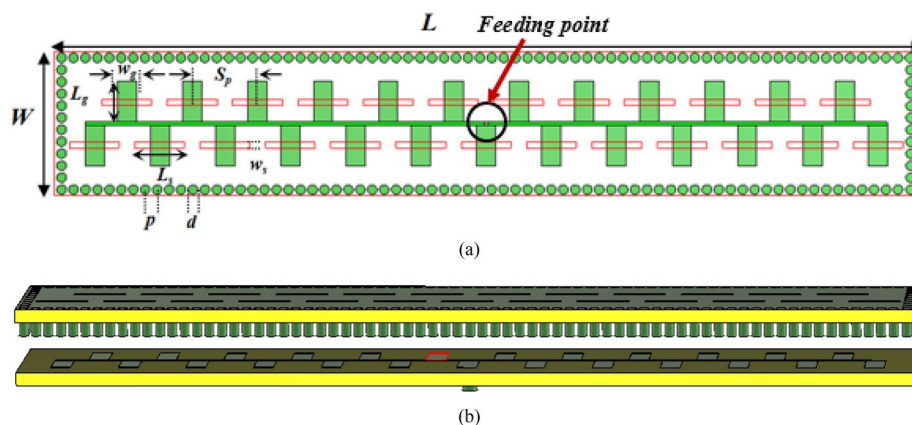
### Design configuration

Figure 2a and b illustrates the suggested antenna configuration, comprising two Rogers 5880 substrates with a thickness of 1.578 mm and a permittivity of 2.2. Twenty-five radiating slots are positioned on the top layer of the first substrate to meet the radiation pattern requirements specified for automotive radar applications.

The radiating slots have a symmetrical arrangement along both the x and y axes, with symmetrical excitation of phase and amplitude around the origin. To achieve a low SLL, the inter-element spacing is optimized to  $\lambda/2$  between the SAA elements. These elements are positioned to realize optimal performance. The upper layer of the bottom substrate introduces a new configuration for the feeding network. The unique grid-feeding configuration with center excitation contributes to high gain and a low profile design.

The SIW cavity backing is employed to minimize surface wave currents, resulting in SLL values in both the XZ plane and YZ plane of less than  $-23$  dB. The dimensions of the conductive vias and their periodicity in the SIW are designed to match the desired frequency band of the radiating slots, following the equations outlined in [32]. The optimized via dimensions are as follows: via width ( $d$ ) = 1 mm, via period ( $p$ ) = 2.7 mm, and via height ( $h$ ) = 6.25 mm.

To validate the optimized interspacing between the SAA elements, the electric field distribution of the radiating slots is depicted in Fig. 3. It is evident that the slots exhibit an in-phase current, which is augmented in the broadside direction, resulting in high gain. However, surface waves remain a concern, contributing to a high SLL, as shown in Fig. 4a. Conversely, when using an SIW, the array slots are embedded in a dielectric substrate, confining the electric field within itself and creating a guided mode, as illustrated in Fig. 4b. The use of SIW enhances the efficiency and directivity of the SAA while



**Fig. 2** The proposed planar slot antenna array (SAA) **a** Antenna configuration top, **b** side view

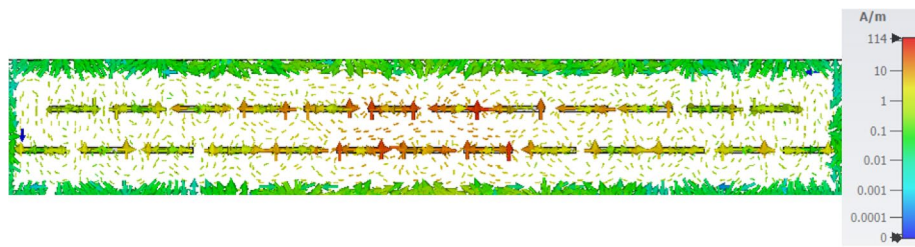


**Fig. 3** The current distribution of the proposed planar slot antenna array (SAA)

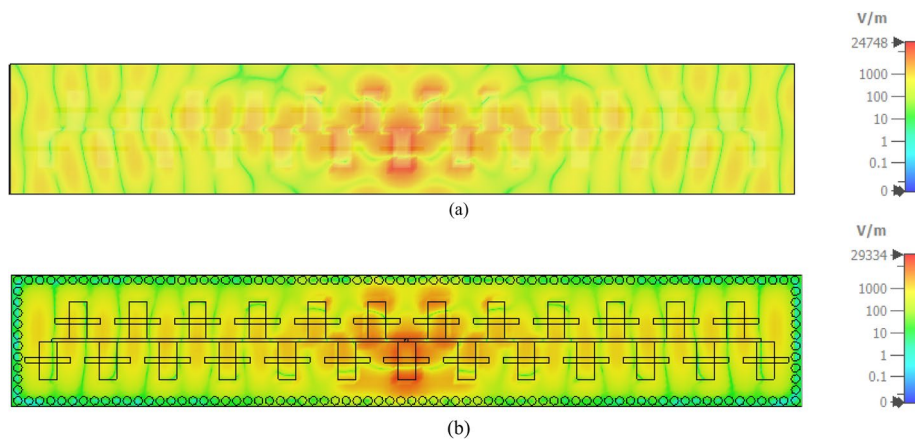


**Fig. 4** The electric field of the proposed planar SAA **a** Without SIW. **b** With SIW

**Table 1** The proposed antenna dimensions in Mm

$L$	$W$	$L_s$	$W_s$	$L_g$	$W_g$	$S_p$	$P$	$d$
108.5	18	6.25	0.75	5.13	2.4	8.2	1.5	1.2

reducing leakage and increasing the antenna gain. The optimized dimensions of the proposed antenna are detailed in Table 1.

**Design procedures**

The design procedure of the SAA under consideration is characterized by a comprehensive approach aimed at optimizing its performance for automotive radar applications. The subsequent subsections will detail the sequential steps we followed to arrive at the final design, unraveling the intricacies of our methodology and decision-making process.

**Design of slot element**

The central element of the proposed linear antenna array is the radiating slot, characterized by its length “ $l_s$ ” and spacing “ $S_p$ .” It is essential that the length “ $l_s$ ” and the spacing “ $S_p$ ” are chosen to be approximately  $\lambda_g/2$  and  $\lambda_0/2$ , where  $\lambda_0$  and  $\lambda_g$  represent the free space and guided wavelengths, respectively. The offset of each slot from the center line is denoted by “ $x_0$ .” The width “ $w_s$ ” of the slots should be chosen as a small fraction of the wavelength, typically  $\lambda_0/10$ , considering each radiating slot as a magnetic dipole.

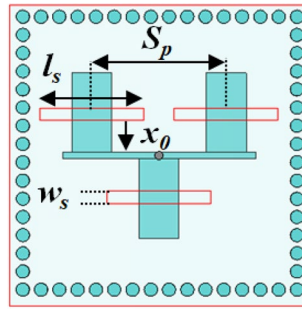


**Fig. 5** The simulated VSWR versus frequency

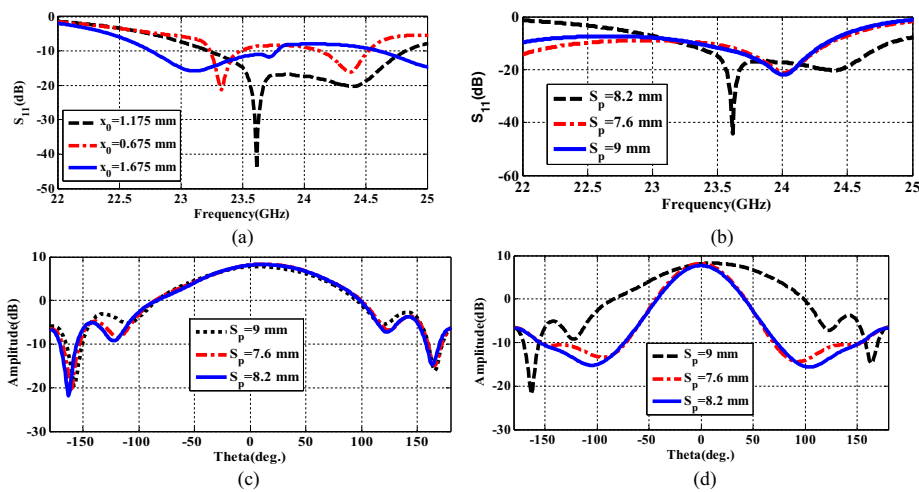


**Fig. 6** The 3-elements SAA. **a** Reflection coefficients with different slot offset, **b** Reflection coefficients, **c** E-plane, and **d** H-plane with different slot separation

Proper adjustment of the slots width and thickness is essential as it can influence impedance matching. To illustrate the operating principle of the slot element, three elements are initially designed and excited using a straightforward grid array feeding network, as depicted in Fig. 5. It is essential to emphasize that the optimal spacing between slots in an SAA depends on a number of factors, including the intended radiation characteristics, operating frequency, and specific antenna design objectives. In closely spaced SAA, electromagnetic coupling can occur between adjacent slots, resulting in cross talk that can affect the radiation pattern and overall array performance. Additionally, the spacing between slots plays a significant role in influencing the presence and magnitude of side lobes in the radiation pattern. A judicious choice of spacing can effectively minimize SLL, mitigating undesired radiation in certain directions. Figure 5 presents the reflection coefficients and radiation patterns at 24 GHz for different slot spacings. In Fig. 6a, the reflection coefficients for various slot offsets from the center line “ $x_0$ ” are shown, highlighting the significant impact of slot offset on impedance matching. Additionally, Fig. 6b illustrates a satisfactory match below  $-10$  dB within the desired frequency range for different slot spacings. On the other hand, Fig. 6c and d depicts the radiation patterns in the E-plane and H-plane, respectively. The results indicate that as the distance

between the slots increases, the radiation pattern becomes narrower and more focused, with minimal SLL. This configuration results in increased gain and concentrated coverage in a specific direction.

### **Feeding network**

The proposed SAA introduces the use of the grid configuration as a means of providing excitation to the SAA elements, rather than using it solely for radiation purposes [31]. Traditionally, the grid array is fed near its center for optimal performance. Grid feeding is particularly suitable due to the uniform phase degradation of electromagnetic waves as they propagate from the feeding point toward the outer edges of the radiating array. In this configuration, the grid elements also carry in-phase current to facilitate effective excitation. Figure 7 depicts the structure of the grid feed network and the distribution of its electric field. Notably, the electric field reaches its maximum intensity at the feeding point and gradually decreases as one moves away from it.

### **Determining the effective number of elements**

The effect of increasing the number of elements on the antenna performance was investigated until reaching the final design. Figure 8a shows the reflection coefficients of configurations with nine, seventeen, and twenty-five elements are presented. All three configurations exhibit good matching (below  $-10$  dB) within the required band. Additionally, their radiation patterns in both the E-plane and H-plane are illustrated in Fig. 8b and c. The radiation pattern of the 25-element configuration indicates a HPBW of  $12.1^\circ$  in the E-plane and  $69.1^\circ$  in the H-plane, with an SLL of  $-23$  dB in the E-plane. Furthermore, it was observed that the gain increases with the number of elements until it reaches a maximum of 14 dB at 24 GHz (25 elements), all within a compact size of  $108.5 \times 18$  mm<sup>2</sup>.

### **Experimental results of the SAA**

In order to verify the accuracy of the simulated outcomes, we constructed and examined a prototype of the suggested SAA antenna, as displayed in Fig. 9. The comparison between the simulated and measured outcomes of the fabricated antennas can be seen in Fig. 10. A vector network analyzer (VNA) was employed to measure the input reflection coefficient for the proposed SAA array antenna. The simulated frequency band with a VSWR less than two ranged from 23.805 to 24.429 GHz (2.59%), while the measured frequency band in the same condition spanned from 23.851 to 24.840 GHz (4.06%). The simulated and measured results show a small variation in bandwidth. This difference is mainly due to the soldering of the connectors and errors in the manufacture of the PCB. These issues can lead to frequency changes

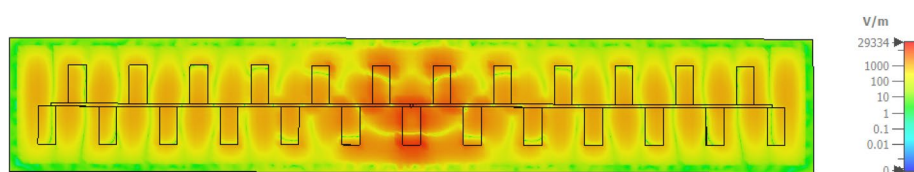


**Fig. 7** Electric field distribution



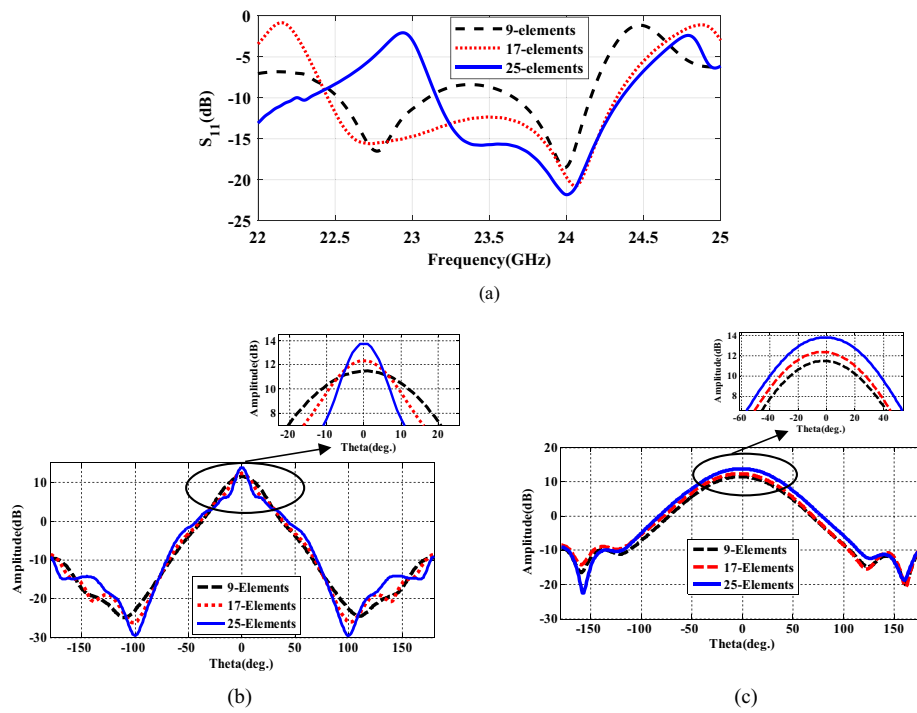


**Fig. 8** The three configurations planar slot antenna array (SAA) **a** Reflection coefficients **b** E-plane **c** H-plane

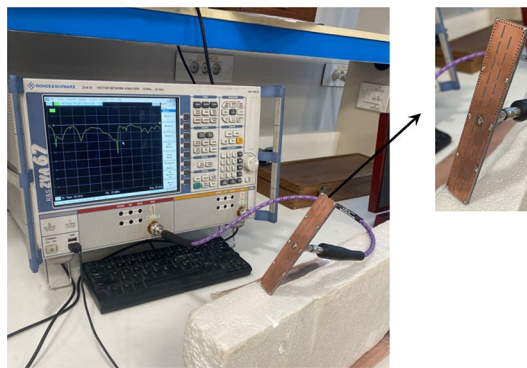


**Fig. 9** Fabricated prototypes of proposed SAA antenna

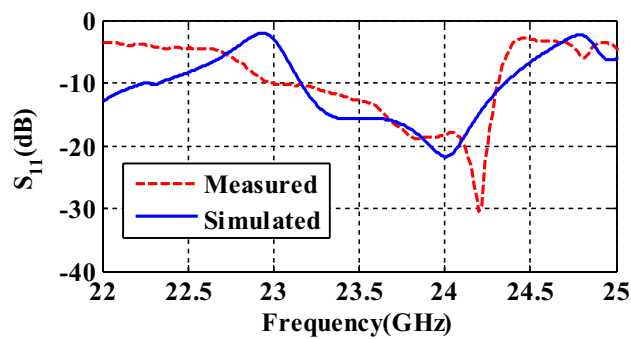


**Fig. 10** Measured and simulated reflection coefficient for the proposed SAA

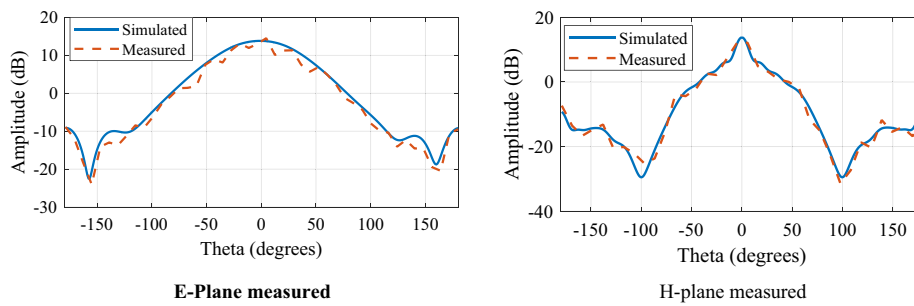


**Fig. 11** Measured and simulated radiation pattern at 24 GHz for the proposed SAA

**Table 2** Comparison with the state-of-art work

References	Frequency	SLL (dB)	Features	Size	Impedance B.W (%)	Peak gain (dBi)	Elements no.
[35]	24 GHz	-14	E-shaped	N/A	4.17	25.2	64
[36]	24 GHz	-20	Series-fed array	N/A	1.03	14.5	N/A
[37]	24 GHz	-15	Patch	N/A	8.3	12.5	8
[38]	24 GHz	N/A	Waveguide parasitic	18 mm × 19.6 mm	1.31	10.3	9
[39]	28 GHz	-2.6	Vivaldi array	33.31 mm × 54.96 mm	17.47	11	8
[40]	15 GHz	-23	Slot array	N/A	3.5	20	40
Our work	24 GHz	-23	Slot array	108 mm × 18 mm	5.49	14	25

and signal loss, particularly at mm-wave frequencies [33, 34]. To assess the radiation pattern, a proposed antenna was employed as the receiving component and a conventional mm-wave horn antenna served as the transmitting component. The transmitting and receiving antennas were positioned at least one wavelength apart. In order to accurately estimate the gain, both antennas had to be exposed to a uniform plane wave, i.e., any reflections or transmissions had to be minimized. In order to avoid any unwanted interference, mm-wave absorbers were placed around the measurement equipment. The radiation characteristics of the antenna were assessed using the gain transfer technique, and the results can be seen in Fig. 11 [34]. A clear correlation can be observed between the simulations and the measurements. However, slight variations were observed in the measured results due to manufacturing tolerances, the presence of the VNA, and the metallic antenna holders inside the chamber.

Table 2 in this paper compares the features of the proposed antenna with previous works. It is observed that the SLL achieved in this paper is about 9 dB lower compared to those achieved in [35] and [38]. However, the SLL obtained in [39] is considerably high, the gain is slightly lower than that of the proposed work. In [36], the gain and SLL are satisfactory but the impedance bandwidth is relatively low. This paper presents a good characteristic with a low SLL. It is evident that the combination of

very low SLL, stable broadside radiation, and high gain makes the proposed structure appealing for radar applications.

### Proposed MIMO radar

#### MIMO antenna configuration

The 20 elements of the proposed radar system—7 transmitters and 13 receivers—are arranged to synthesize 91 densely virtual units. Figure 12a shows this configuration. The number of antenna elements has been chosen to ensure that at a minimum height of 5 m, the radar sensor design avoids any reflections from roadside traffic signs or bridges in the vertical direction. A fairly large beamwidth of around 70° in the azimuth direction is required to detect neighboring pathways. To attain a low SLL for a certain MIMO design arrangement, it is recommended that the Tx array factor has nulls at each grating lobe of Rx, and vice versa, based on Eq. 1. For this reason, the spacing between the Tx elements is set to  $1.5 \lambda_0$  and  $6 \lambda_0$  for Rx, as shown in Fig. 12a. Figure 12b shows the array factor of the suggested configuration. The virtual array’s SLL is less than  $-15$  dB within the effective angle of monitoring ( $-40^\circ$  to  $40^\circ$ ), where the  $AF_{Tx}$  nulls cancel out the  $AF_{Rx}$  grating lobe, when this suggested MIMO

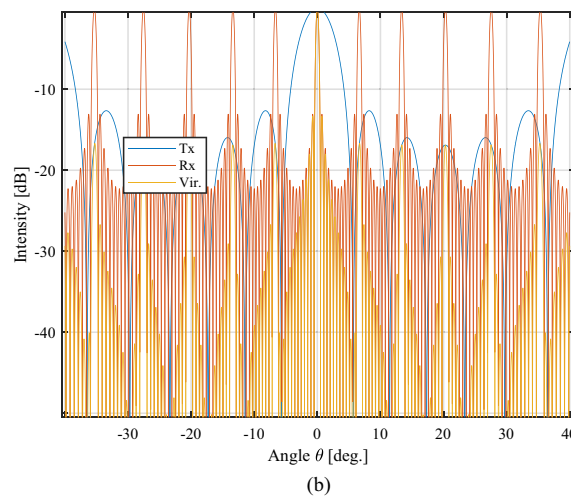
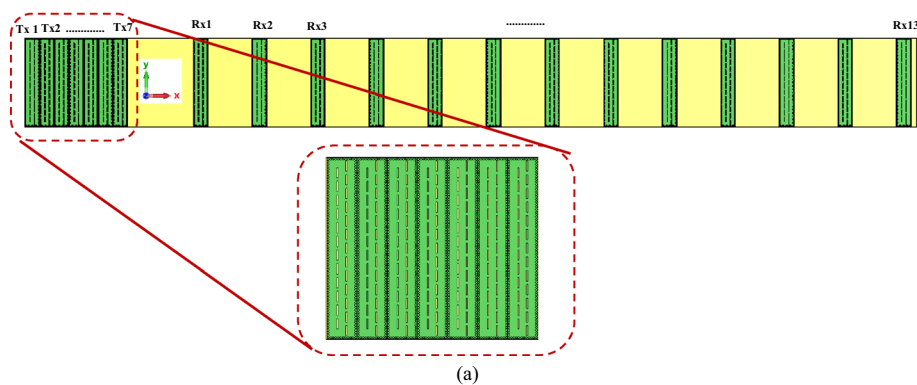


**Fig. 12** MIMO antenna configuration **a** MIMO configuration. **b** MIMO radiation pattern array factor

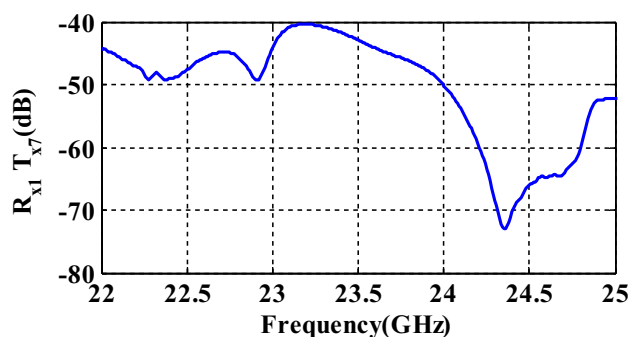


**Fig. 13** The MIMO elements mutual coupling

configuration is used. Figure 13 examines and displays the coupling between the closest Tx-Rx antennas, demonstrating exceptional isolation of more than 40 dB.

### **Radar image reconstruction**

To validate the proposed MIMO configuration in a radar application, the antenna is simulated as part of a MIMO radar system. The following is a summary of the steps involved in designing a linear uniform array. First, find the bandwidth of the SFCW B using  $\delta_r = c/2B$ , considering the range resolution requirement  $\delta_r$ . Second, get the array length using  $L = \lambda R_0 \delta_a$ , where  $\lambda = c/f_H$  is the wavelength and  $f_H$  is the maximum frequency, and the required azimuth resolution  $\delta_a$  for the given range  $R_0$ . Thirteen RX and seven TX antennas make up the planned radar. With a central frequency of 24 GHz (K-band), the SFCW radars will transmit 2048 frequencies within a 500 MHz spread. The azimuth angular resolution of the radar is  $0.2^\circ$ , and its maximum range ambiguity is 613 m. In [31], the specifics of the used signal processing methodology are explained. The simulated radar image acquired using the characteristics of a MIMO automotive radar system is displayed in Fig. 14. The position of the nine targets is in meters and they are located at  $(x, y)$  positions of (0, 4), (0, 4.5), (0, 5), (0, 5.5), (0, 6), (1, 5), (0.5, 5), (-0.5, 5), and (-1, 5) from the radar system. The proposed system that has been suggested has exceptional resolution in both azimuth and range directions, confirming that the suggested configuration is suitable for MIMO radar systems.

### **Conclusion**

This paper introduces a new design for a 24 GHz wideband for radar applications. The design features a unique  $50 \Omega$  center excitation grid feed configuration for the SAA. Unlike conventional microstrip patch antennas, the proposed array antenna utilizes a slot-loaded technique to enhance the bandwidth, resulting in a wider bandwidth. The working principle of the grid array for feeding the SAA is then demonstrated. In addition, this paper presents the use of the SIW technique to achieve low sidelobe level and high gain. The proposed antenna has a peak gain of 14.2 dBi and a low SLL of  $-23$  dB, as well as a fanbeam radiation pattern with specific angles of  $\theta_E = 12.1^\circ$  and  $\theta_H = 69.1^\circ$ , and an impedance bandwidth of 5.49% at 24 GHz. Overall, the designed and realized SAA is specifically tailored to meet the requirements of radar applications.

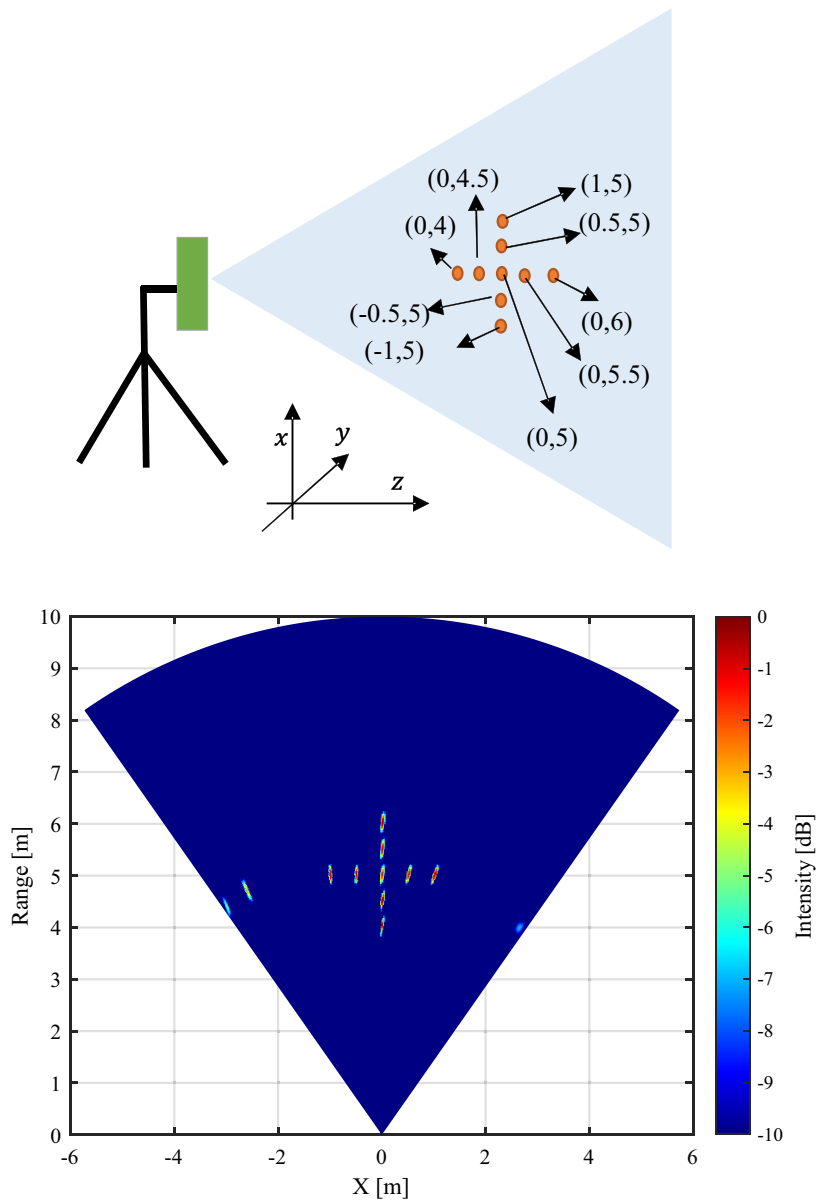


**Fig. 14** Automotive Radar short-range image of two targets in different azimuth and range locations

**Abbreviations**

- SAA Slot antenna array
- SLL Side lobe level
- SIW Substrate-integrated waveguide
- HPBW Half-power beamwidth
- MIMO Multi-input multi-output
- CW Continuous-wave
- FMCW Frequency-modulated CW
- FSK Frequency shift keying
- VCO Voltage-controlled oscillator
- VNA Vector network analyzer

**Author contributions**

S.M. was involved in conceptualization; A.S. helped in methodology; investigation was done by S.M. and A.S.; E.O. helped in writing—original draft preparation; S.M., E.O., and A.S. helped in writing—review and editing; supervision was done by S.M. All authors have read and agreed to the published version of the manuscript.

**Funding**

This research received no external funding.

**Availability of data and materials**

The original contributions presented in the study are included in the article, further inquiries can be directed to the corresponding authors.

**Declarations****Competing interests**

The authors declare no conflicts of interest.

Received: 2 July 2024 Accepted: 7 August 2024

Published online: 03 September 2024

**References**

- Skolnik F, Merrill I (1962) Introduction to radar: radar handbook. McGraw-Hill, New York
- James RJ (1989) A history of radar. *IEE Rev* 35:343–349
- Greco MS, Li J, Long T, Zoubir A (2019) Advances in radar systems for modern civilian and commercial applications. *IEEE Signal Process Mag* 36(4):13–15
- Lin J, Li C, Chang CC, Tsai T, Zito D, Chang SF (2018) Review—Semiconductor integrated radar for sensing applications. *ECS J Solid State Sci Technol* 7:3126–3142
- Liang T, Liu R, Yang L, Lin Y, Shi CJR, Xu H (2024) Fall detection system based on point cloud enhancement model for 24 GHz FMCW radar. *Sensors* 24:648
- Yang K, Kim M, Jung Y, Lee S (2024) Hand gesture recognition using FSK radar sensors. *Sensors* 24:349
- Xu L, Sun S, Mishra KV, Zhang YD (2023) Automotive FMCW radar with difference co-chirps. *IEEE Trans Aerosp Electron Syst* 59:8145–8165
- Abd El-Hameed AS, Sato M (2022) Evaluation of 79 GHz MIMO radar under sandy conditions in Egypt. In: *IEEE international geoscience and remote sensing symposium*, pp 7483–7486
- Kumar A, Gautam SK, Arya RK, Ali M, Singh PP, Verma AK, Mittra R (2024) High-gain TM<sub>11</sub> mode equilateral triangular patch antenna with shorting pins and triangular short horn. *Int J Microw Wirel Technol* 200:1–15. <https://doi.org/10.1017/S1759078724000382>
- Ou JH, Huang J, Liu J, Tang J, Zhang XY (2020) High-gain circular patch antenna and array with introduction of multiple shorting pins. *IEEE Trans Antennas Propag* 68:6506–6515
- Ding K, Gao C, Yu T, Qu D, Zhang B (2016) Gain-improved broadband circularly polarized antenna array with parasitic patches. *IEEE Antennas Wirel Propag Lett* 16:1468–1471
- Koul SK, Swapna S, Karthikeya GS (2024) Antenna gain enhancement techniques. *Antenna Systems for modern wireless devices*. Springer, Singapore, pp 153–188
- Karthigaiveni S, Reddy MA, Pandeewari R (2023) Aperture coupled four element MIMO antenna loaded with NBSRR superstrates for 5G wireless communications. *Wirel Pers Commun*. <https://doi.org/10.1007/s11277-023-10359-7>
- Tewary T, Maity S, Mukherjee S, Roy A, Sarkar PP, Bhunia S (2021) Design of high gain broadband microstrip patch antenna for UWB/X/Ku band applications. *AEU Int J Electron Commun* 39:153905
- Ibrahim AA, Ali WA (2021) High gain, wideband and low mutual coupling AMC-based millimeter wave MIMO antenna for 5G NR networks. *AEU Int J Electron Commun* 142:153990
- Lavadiya SP, Patel SK, Maria R (2021) High gain and frequency reconfigurable copper and liquid metamaterial tooth based microstrip patch antenna. *AEU Int J Electron Commun* 137:153799
- Cao W, Zhang B, Liu A, Yu T, Guo D, Wei Y (2012) Gain enhancement for broadband periodic endfire antenna by using split-ring resonator structures. *IEEE Trans Antennas Propag* 60(7):3513–3516
- Dadgarpour A, Kishk AA, Denidni TA (2016) Gain enhancement of planar antenna enabled by array of split-ring resonators. *IEEE Trans Antennas Propag* 64(8):3682–3687
- Xu HX, Tang S, Wang GM, Cai T, Huang W, He Q et al (2016) Multifunctional microstrip array combining a linear polarizer and focusing metasurface. *IEEE Trans Antennas Propag* 64:3676–3682
- Xu HX, Cai T, Zhuang YQ, Peng Q, Wang GM, Liang JG (2017) Dual-mode transmissive metasurface and its applications in multibeam transmitarray. *IEEE Trans Antennas Propag* 65(4):1797–1806
- Zhou H, Hong W, Tian L, Cheng L (2016) Cross-polarization suppressed and linearly polarized patch array antenna with cavity-backed slot feed for vehicle applications. *IEEE Antennas Wirel Propag Lett* 15:126–129
- Han L, Wu K (2012) 24-GHz bandwidth-enhanced microstrip array printed on a single-layer electrically-thin substrate for automotive applications. *IEEE Trans Antennas Propag* 60(5):2555–2558
- Xu J, Chen ZN, Qing X (2014) CPW center-fed single-layer SIW slot antenna array for automotive radars. *IEEE Trans Antennas Propag* 62(9):4528–4536
- Agrawal N, Gautam AK, Rambabu K (2020) Design and packaging of multi-polarized triple-band antenna for automotive applications. *AEU Int J Electron Commun* 113:152943
- Chen Z, Ping ZY (2015) 24-GHz microstrip grid array antenna for automotive radars application. In: *2015 IEEE 5th Asia-Pacific conference on synthetic aperture radar (APSAR)*, pp 125–127
- Richardson PN, Lee HY (1988) Design and analysis of slotted waveguide arrays. *Microw J* 31:109–125
- Hirokawa J, Ando M (2000) 45 linearly polarized post-wall waveguide-fed parallel-plate slot arrays. *IEE Proc Microw Antennas Propag* 147(6):515–519

28. Yan L, Hong W, Hua G, Chen J, Wu K, Cui TJ (2004) Simulation and experiment on SIW slot array antennas. *IEEE Microw Wirel Compon Lett* 14(9):446–448
29. Park S, Okajima Y, Hirokawa J, Ando M (2005) A slotted post-wall waveguide array with interdigital structure for 45° linear and dual polarization. *IEEE Trans Antennas Propag* 53(9):2865–2871
30. Chen ZJ, Hong W, Kuai ZQ, Tang HJ, Chen JX (2007) 45° linearly polarized resonant slot array antenna based on substrate integrated waveguide. In: *Asia-Pacific microwave conference*, vol 3, pp 1551–1555
31. Abd El-Hameed AS, Ouf EG, Elboushi A, Seliem AG, Izumi Y (2023) An improved performance radar sensor for K-band automotive radars. *Sensors* 23:7070
32. El-Nady S, Elsharkawy R, Afifi AI, Abd El-Hameed AS (2021) Performance improvement of substrate integrated cavity fed dipole array antenna using ENZ metamaterial for 5G applications. *Sensors* 22:125
33. Al-Tarifi MA, Anagnostou DE, Amert AK, Whites KW (2013) Bandwidth enhancement of the resonant cavity antenna by using two dielectric superstrates. *IEEE Trans Antennas Propag* 61(4):1898–1908
34. Eid R, Elboushi A, Hindy M (2021) Wideband monopole antenna with multiple stub resonators for 5G applications. In: *38th national radio science conference (NRSC)*, pp 80–87
35. Shan J, Rambabu K, Zhang Y, Lin J (2022) High gain array antenna for 24 GHz FMCW automotive radars. *AEU Int J Electron Commun* 147:154144
36. Wang Y, Wang X, Yuan F (2022) Design and implementation of 24GHz series fed microstrip antenna array for automotive radar. In: *2022 14th international conference on measuring technology and mechatronics automation (ICMTMA)*, pp 887–890
37. Slomian I, Wincza K, Gruszczynski S (2013) Low-cost broadband microstrip antenna array for 24 GHz FMCW radar applications. *Int J RF Microw Comput Aided Eng* 23(4):499–506
38. Deckmyn T, Caytan O, Bosman D, Lima de Paula I, Van Messem L, Rogier H et al (2018) Single-fed 3 × 3 substrate-integrated waveguide parasitic antenna array for 24 GHz radar applications. *IEEE Trans Antennas Propag* 66(11):5955–5963
39. Ullah R, Ullah S, Faisal F, Ullah R, Choi DY, Ahmad A, Kamal B (2021) High-gain vivaldi antenna with wide bandwidth characteristics for 5G mobile and Ku-Band radar applications. *Electronics* 10:667
40. Ghorbani S, Razavi SA, Ostovarzadeh MH, Farahbakhsh A (2020) Development of a center fed slot array antenna with very low side lobes using ridge gap waveguide (RGW) technology. *AEU Int J Electron Commun* 125:153385

### Publisher's Note

Springer Nature remains neutral with regard to jurisdictional claims in published maps and institutional affiliations.